Vibration of microperforated plate with spatial distribution of multiple-sized perforations

Lucie Gallerand, Mathias Legrand, Thomas Dupont, Philippe Leclaire

inter·noise 2023
CHIBA,GREATER TOKYO 20-23 AUGUST

Vibration of microperforated plate with spatial distribution of multiple-sized perforations

Lucie Gallerand [1]
École de technologie supérieure
Montréal, Canada

Mathias Legrand
McGill University
Montréal, Canada

Thomas Dupont
École de technologie supérieure
Montréal, Canada

Philippe Leclaire
Université de Bougogne
Nevers, France

ABSTRACT

Recent works by the authors on homogeneous MPPs have highlighted the structural damping capabilities of MPPs in the low frequency range. The developed theoretical approach was based on the analogy between an MPP and a porous plate. The added damping is due to visco-thermic effects coupled to fluid-structure interactions. The added damping maxes out at a characteristic frequency depending on perforation diameter. In order to reduce plate vibrations, it was advised to match the characteristic frequency to a plate mode. It is proposed here to maximize the added damping effect on several vibration modes by focusing on MPPs with multiple-sized perforations and with spatial distribution of perforations. As an extension of the previous analytical model, an approach based on the electro-acoustic analogy is established to capture the effect of multiple-sized perforations. Moreover, a perforation ratio gradient is included in the approach to model an MPP with inhomogeneous spatial distribution of perforations. Experimental measurements on MPPs validate the proposed analytical model. Results show that: (i) MPP with multiple-sized perforations increases the frequency band of the effective damping; (ii) the added damping increases when the perforations are distributed around the antinodes of the considered mode, (iii) the two effects can be combined.

1. INTRODUCTION

Microperforated plates (MPP) are widely used structures in the field of acoustics. These simple structures are simple, lightweight and are currently used in many industrial fields such as the transport sector. For example, MPP is used as acoustic absorber in launcher fairings [1]. Models characterizing

[1] lucie.gallerand.1@ens.etsmtl.ca

the acoustic absorption of these structures have been proposed: (1) models based on the Kirchhoff equations [2]; (2) models based on fluid-equivalent method using Johnson-Allard approach [3, 4]. In order to improve the sound absorption of MPPs in this acoustic context, some research works have proposed different MPP designs. In this way, different configurations of MPP with multi-sized perforation were proposed [5, 6]. Electro-acoustic model was used by Qian *et al.* [7]. Experimental investigation on the sound absorption performance of an MPP with multi-sized perforation was also performed by Miasa *et al.* [5]. Their results showed that multi-sized MPP absorbers can exhibit high sound absorption over a wider frequency range than uniformly sized MPPs. On another way, Temiz *et al.* [8] explored numerically the effect of spatial distribution of perforation on sound absorption by assuming a discrete impedance patches model [9, 10]. They noted that the distribution of perforations on the MPP could have a substantial effect on the viscous damping mechanism.

On the other hand, the authors were recently interested on the dynamic behaviour of these structures in a previous work [11]. They showed that the MPP exhibited additional damping in the low frequency range. They showed that this effect was maximal at a characteristic frequency and that it acted on a range of surrounding frequencies. However, this previous study was done for MPPs with a single set of perforations and with homogeneous perforation distributions.

In this paper, it is proposed: (i) to maximize the added damping by using a spatial perforation distribution, (ii) to widen the frequency band of effective damping by different sized of perforation spatial distributed on MPP surface. To this end, Section 2 recalls the analytical model proposed by the authors in [11] while Section 3 proposes an analytical model to capture the effect of MPP with multiple spatially distributed perforations on the plate response based on the combination of: (i) a homogenization approach for MPP with multi-sized perforations; (ii) a model definition of a spatial perforation ratio. The models and analyses proposed in the rest of the paper will be detailed in a future publication submitted in May 2023 [12].

2. STRUCTURAL DYNAMIC OF FINITE-SIZE MPP

2.1. Governing equations: general case

Based on an alternative form of Biot's theory, an analytical model of the vibration of a finite size MPP is developed by the authors [11] by identifying the MPP with an equivalent porous plate an [4]. The resulting equations are based on [13] and take the form of the following coupled system :

$$\Big(D + \frac{\alpha^2 M_\mathrm{f} h^3}{12}\Big)\nabla^4 w_\mathrm{s}(x,y,t) + h(\rho \ddot{w}_\mathrm{s}(x,y,t) + \rho_\mathrm{f}\ddot{w}(x,y,t)) = f_\mathrm{ext}(x,y,t), \tag{1a}$$

$$\alpha M_\mathrm{f}\nabla^2 w_\mathrm{s}(x,y,t) + \Big(\rho_\mathrm{f}\ddot{w}_\mathrm{s}(x,y,t) + \frac{\rho_\mathrm{f}\alpha_\infty}{\phi^{(0)}}\ddot{w}(x,y,t)\Big) + \sigma^{(0)}\dot{w}(x,y,t) = 0, \tag{1b}$$

with ∇ is the differential operator defined so that $\nabla^2(\cdot) = \frac{\partial^2(\cdot)}{\partial x^2} + \frac{\partial^2(\cdot)}{\partial y^2}$ and $\nabla^4(\cdot) = \nabla^2(\cdot)^2$. The external load is noted $f_\mathrm{ext}(x,y,t)$. Equation 1 are obtained under the low-frequency assumption for a finite-size MPP saturated by a light fluid. The MPP is here considered as two equivalent homogeneous plates: (1) an equivalent solid plate without perforations with equivalent bending stiffness coefficient D and equivalent density of fluid-solid mixture ρ; (2) an equivalent fluid plate which corresponds to the fluid present in the microperforations. Solving Equation 1 lead to the solid displacement $w_\mathrm{s}(x,y,t)$ and the relative fluid-solid motion $w(x,y,t)$. Equation 1a corresponds to the elastic response of the equivalent non-perforated homogeneous solid plate, and Equation 1b to the coupling fluid-solid. JCA (Johnson-Champoux-Allard) macroscopic parameters such as airflow resistivity $\sigma^{(0)}$, porosity called perforation ratio in an MPP case $\phi^{(0)}$ and tortuosity α_∞ are adapted to the case of a microperforated plate and are only a function of perforation diameter $\sigma^{(0)}$. In this context, the airflow resistivity writes

$$\sigma^{(0)} = \frac{\varsigma}{\phi^{(0)}} \quad \text{with} \quad \varsigma = \frac{32\mu_\mathrm{f}}{d^2}. \tag{2}$$

In addition, to account for fluid distortion at the perforation end and perforation interaction, an empirical correction is applied to the tortuosity, which is rewritten [4]

$$\alpha_\infty = 1 + B(1 - 1.14\sqrt{\phi^{(0)}}) \quad \text{with} \quad B = \frac{0.48}{h}\sqrt{\pi d^2}. \tag{3}$$

In order to consider the effect of the microperforation on the plate response, bending stiffness is adapted and become a $\phi^{(0)}$-function. The bending stiffness therefore depends on $\phi^{(0)}$ as follows:

$$D = \frac{Eh^3}{12(1-\nu^2)}\frac{(1-\phi^{(0)})^2}{1+(2-3\nu)\phi^{(0)}}. \tag{4}$$

where E is the non-perforated plate Young modulus and ν the Poisson's coefficient. For an MPP saturated by a light fluid, the density of the fluid-solid mixture is also written as a function of the perforation ratio, such that $\rho = \rho_\mathrm{s}(1-\phi^{(0)})$.

Equation 1 are solved by a modal analysis, the reader is invited to refer to [11, 12] for more information on the resolution procedure.

2.2. Biot's frequency and maximum added damping

Fluid-solid interactions coupled with visco-thermal interactions in the boundary layers of microperforations lead to substantial added damping as exhibited by [11]. These dissipation mechanisms involved in an MPP reach a maximum at the particular characteristic frequency already defined in the context of porous materials [13, 14]. The characteristic frequency

$$f_\mathrm{c} = \frac{32\mu_\mathrm{f}}{2\pi\alpha_\infty\rho_\mathrm{f}d^2} \tag{5}$$

is only a function of perforation diameter d and the fluid parameters ρ_f and μ_f. The added damping provided by the MPP can be maximized at a particular resonance frequency by matching the natural resonance frequency of the plate with f_c through adjustment of the perforation diameter. The added damping is maximal at f_c but acts on a range around this characteristic frequency.

3. ADDED DAMPING MAXIMIZATION

In this section, the added damping effect is maximized by proposing design of MPP in each section. In Section 3.1, the frequency band of effective damping is widened by using an MPP with multi-sized of perforation. In Section 3.2, the added damping is maximized on a particular mode by using spatial distribution of perforations. In Section 3.3, an MPP combining the both effect is proposed.

3.1. MPP with multi-size perforation diameter: analytical model

The added damping presented by the MPP is closely related to the diameter of the perforation, which when properly chosen reduces the vibrations around a resonance frequency of the plate. Using an MPP with several perforation diameters would increase the frequency range where the added damping is significant. This is the reason why, a multi-sized perforation MPP with N different perforation diameters denoted d_k with $k = 1, 2, \cdots, N$ is considered. The vibratory response of an MPP with multi-sized perforation is model by using a homogenization procedure. In this context, $2N$ equivalent plate is defined in the same mathematical spatial domain: (1) N equivalent homogeneous solid plate; (2) N equivalent homogeneous fluid plate. An example of an MPP with two perforation diameters, i.e. $N = 2$ is given in Figure 1. Each equivalent plate is related to its perforation ratio $\phi_k^{(0)}$ and its

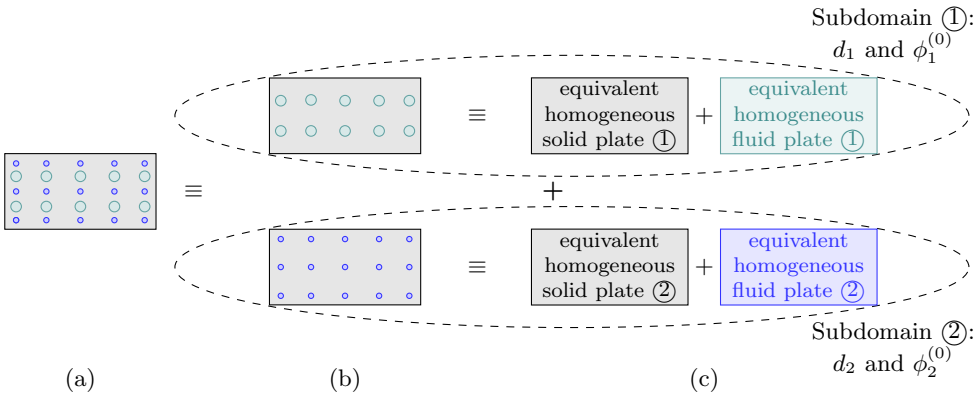

Figure 1: MPP with two perforation diameters. The MPP given in (a) is decomposed into two MPPs each associated with a diameter and a perforation ratio as shown in (b). Each MPP of (b) through a homogenization approach is equivalent to two plates, one of equivalent fluid and one of equivalent solid, as shown in (c).

perforation diameter d_k. The overall perforation ratio ϕ_{tot} of the MPP writes

$$\phi_{\text{tot}}^{(0)} = \sum_{k=1}^{N} \phi_k^{(0)}. \tag{6}$$

The overall airflow resistivity is defined using a homogenization approach [6, 15, 16]:

$$\frac{1}{\sigma} = \sum_{k=1}^{N} \frac{1}{\sigma_k}, \tag{7}$$

where σ_k is obtained through Equation 2 applied on d_k. The bending stiffness is defined as a function of ϕ_{tot}. Equation 6 and Equation 7 are inserted in Equation 1 to obtain the response of an MPP with multi-sized perforation diameter.

3.2. MPP with spatial distribution: analytical model

The additional damping is due to relative movement between the fluid in the perforation and the structure. The more relative motion there is, the more interaction there is, so to improve the additional damping effect it is possible to concentrate the perforations on the antinodes of the modes whose amplitude is to be reduced. In order to explore the influence of the spatial distribution of perforations on the MPP surface, the model presented in Section 1 is extended by defining the perforation ratio as a spatial function :

$$\phi(x, y) = \phi^{(0)}\, \mathbb{Ih}(x, y). \tag{8}$$

The term $\phi^{(0)}$ is the maximal local perforation ratio obtain when the normalized inhomogeneity function $\mathbb{Ih}(x, y)$ is equal to 1. The perforation ratio become a local variable, and the overall perforation ratio is defined via a surface integral. The bending stiffness coefficient and the tortuosity are also defined as a $\phi(x, y)$-function such as

$$D(x, y) = \frac{Eh^3}{12(1-\nu^2)} \frac{(1-\phi(x,y))^2}{1+(2-3\nu)\phi(x,y)} \quad \text{and} \quad \alpha_\infty(x, y) = 1 + B(1 - 1.14\sqrt{\phi(x, y)}) \tag{9}$$

where B is defined in Equation 3. By injecting Equation 8 and Equation 9 into Equation 1 and replacing $w(x, y, t)$ with its expression $w(x, y, t) = \phi(x, y)[w_{\text{f}}(x, y, t) - w_{\text{s}}(x, y, t)]$, the coupled system becomes:

$$D(x, y)\nabla^4 w_{\text{s}} + h(\rho_{\text{s}}(1-\phi(x, y))\ddot{w}_{\text{s}} + \rho_{\text{f}}\phi(x, y)\ddot{w}_{\text{f}}) = 0, \tag{10a}$$

$$\alpha M_{\text{f}}\nabla^2 w_{\text{s}} + \rho_{\text{f}}((1-\alpha_\infty(x, y))\ddot{w}_{\text{s}} + \alpha_\infty(x, y)\ddot{w}_{\text{f}}) + \varsigma(\dot{w}_{\text{f}} - \dot{w}_{\text{s}}) = 0. \tag{10b}$$

The new coupled system is also solved by modal analysis after an appropriate projection and discretization on the basis of the non-perforate plate.

3.3. Both effect combined: experimental validation

In this section, the models presented in Section 3.1 and Section 3.2 are combined and experimentally validated using 195 mm × 30.7 mm × 1.17 mm MPP samples presented in Figure 2. Four plates are considered: an non-perforated reference plate; two spatially homogeneous MPPs with a single perforation diameter size, MPP ① associated with $d_1 = 1.3\,\text{mm}$ and $\phi^{(0)} = 10\,\%$ and MPP ② associated with $d_2 = 0.7\,\text{mm}$ and $\phi^{(0)} = 10\,\%$; MPP ③, whose configuration is explained in the following. MPP ③ has two different sizes of perforation (d_1 and d_2), which are distributed by zone according to the maximum of deflection for the mode 1 for the diameter d_1 mm and for the mode 2 for the diameter d_2 mm. The diameter of the perforation d_1 is fixed in order to maximize the added damping on the resonance frequency of mode 1: f_1. The same is done for d_2 which corresponds to the resonance frequency of mode 2: f_2. The MPP in Figure 2 is decomposed in 3 subdomains each associated with perforation diameter, perforation ratio and inhomogeneity function such that:

$$\phi_1(x) = \phi_1^{(0)}\Pi_1(x) \quad \text{with} \quad \Pi_1(x) = \begin{cases} 1 & \text{if } \frac{x}{L_x} \geq 0.695, \\ 0 & \text{otherwise} \end{cases} \quad \text{and} \quad \phi_1^{(0)} = 33\,\%, \tag{11a}$$

$$\phi_2(x) = \phi_2^{(0)}\Pi_2(x) \quad \text{with} \quad \Pi_2(x) = \begin{cases} 1 & \text{if } \frac{x}{L_x} \geq 0.8, \\ 0 & \text{otherwise} \end{cases} \quad \text{and} \quad \phi_2^{(0)} = 11\,\%, \tag{11b}$$

$$\phi_3(x) = \phi_3^{(0)}\Pi_3(x) \quad \text{with} \quad \Pi_3(x) = \begin{cases} 1 & \text{if } 0.165 \leq \frac{x}{L_x} \leq 0.695, \\ 0 & \text{otherwise} \end{cases} \quad \text{and} \quad \phi_3^{(0)} = 16\,\%. \tag{11c}$$

Experimental measurements are performed with an Oberst test bench[2]. The sample is fixed at $x = 0$

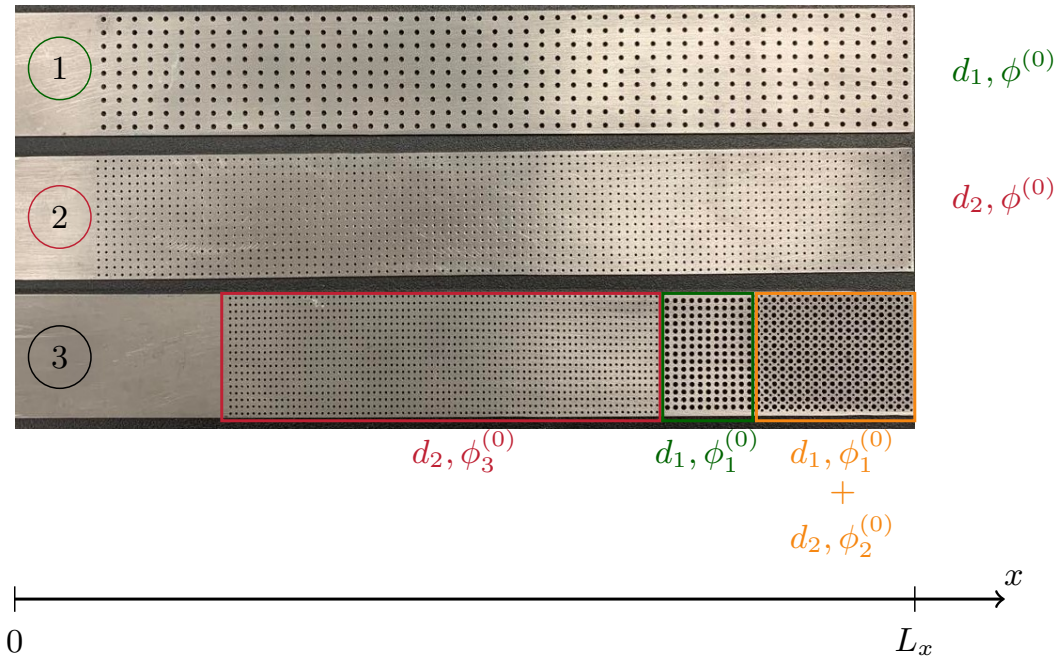

Figure 2: MPP samples used in experimental validation. The spatial distribution of MPP ③ is given in Equation 11.

and excited at $x = L_x$ (see Figure 2). Results are provided in Figure 3. In Figure 3a, the measured

[2]The reader is referred to Section 5 of [11] for more details on the experimental setup.

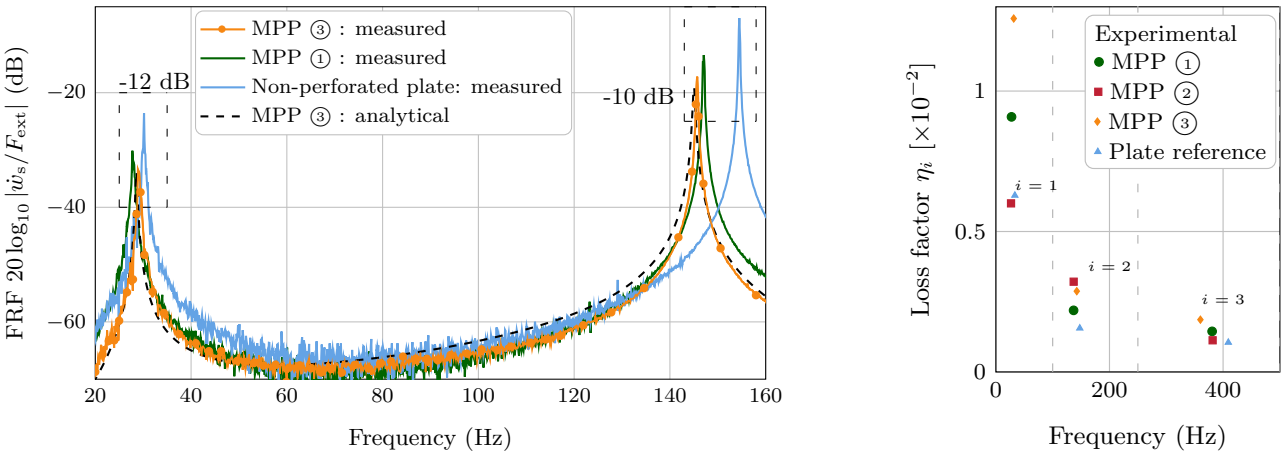

(a) (b)

Figure 3: Experimental measurement of MPP presented in Figure 2. In Figure 3a the experimental and analytical mobility of MPP ③ are compared to this one obtained for the non-perforated case and for the reference MPP case, i.e: MPP ①. In Figure 3b the loss factor of the three MPP of Figure 2 are given for each mode i with $i \leq 4$.

mobility of the MPP is compared to that of the non-perforated plate that acts as reference. In order to validate the analytical model, the experimental results are compared with model results for MPP ③. Figure 3a show that MPP ③ exhibits a magnitude reduction of about 12 dB on the first mode and a magnitude reduction of about 10 dB on the second mode compared to the non-perforated reference plate. In Figure 3b, experimental loss factor for MPP of Figure 2 are given for $i \leq 4$ with $i \in \mathbb{N}$ is the mode index. Results shows that for MPP ③ the loss factor of mode 1 is multiplied by 1.4 compared to MPP ① and by 1.98 compared to the non-perforated plate. The loss factor of mode 2 for MPP ③ is equivalent to that of MPP ② that is multiplied by 1.93 compared to the non-perforated plate case. The use of multiple size microperforations paired with a spatial distribution of perforations has two advantages: (1) depending on the diameters chosen, the additional damping is effective over a wider frequency band compared to a plate with a single set of perforations; (2) the distribution of perforations over the areas of interest also maximizes the additional damping.

4. CONCLUSIONS

This paper is a synthesis of [12] and provides as an extension of [11] analytical models to characterize the vibrational behaviour of MPP with: (i) multi-sized perforation; (ii) spatial distribution of perforation; (iii) a combination of (i) and (ii) that corresponds to an MPP with spatial distribution of multi-sized perforation. Experimental measurements validate the analytical models and show that: (i) MPPs with multiple perforations can broaden the frequency band of effective added damping; (ii) MPPs with spatial distribution of perforations can maximize the added damping on one mode; and (iii) the two effects can add up. For a well-chosen perforation diameter, the frequency band of the effective damping is extended. In addition, the distribution of perforations around the antinodes of the considered mode maximizes the added damping compared to a homogeneous MPP. In practice, it is recommended to concentrate the perforations with an appropriate diameter on the maximum deflection areas of the plate. More details and investigation on each proposed MPP modifications is detailed and more examples are proposed in [12].

REFERENCES

1. S.-H. Park. A design method of micro-perforated panel absorber at high sound pressure environment in launcher fairings. *Journal of Sound and Vibration*, 332(3):521–535, 2013. [DOI].

2. D.-Y. Maa. Potential of microperforated panel absorber. *Journal of the Acoustical Society of America*, 104:2861, 1997. [DOI].
3. Y. Champoux and M.R. Stinson. On acoustical models for sound propagation in rigid frame porous materials and the influence of shape factors. *Journal of the Acoustical Society of America*, 92:1120–1131, 1992. [DOI].
4. N. Atalla and F. Sgard. Modeling of perforated plates and screens using rigid frame porous models. *Journal of Sound and Vibration*, 303:195–208, 2007. [DOI], [OA].
5. I.M. Miasa, M. Okuma, G. Kishimoto, and T. Nakahara. An Experimental Study of a Multi-Size Microperforated Panel Absorber. *Journal of System Design and Dynamics*, 1(2):331–339, 2007. [DOI].
6. K. H. Kim and G. H. Yoon. Absorption performance optimization of perforated plate using multiple-sized holes and a porous separating partition. *Applied Acoustics*, 120:21–33, 2017. [DOI].
7. Y.J. Qian, K. Cui, S.M. Liu, Z.B. Li, D.S. Shao, D.Y. Kong, and S.M. Sun. Optimization of multi-size micro-perforated panel absorbers using multi-population genetic algorithm. *Noise Control Engineering Journal*, 62(1):37–46, 2014. [DOI].
8. M.A. Temiz, J. Tournadre, I.L. Arteaga, P. Martínez-Lera, and A. Hirschberg. Modelling vibro-acoustic coupling in flexible micro-perforated plates by a patch-impedance approach. *Applied Acoustics*, 125:80–90, 2017. [DOI].
9. M. Ouisse, L. Maxit, C. Cacciolati, and J.-L. Guyader. Patch transfer functions as a tool to couple linear acoustic problems. *Journal of Vibration and Acoustics*, 127(5):458–466, 2004. [DOI].
10. L. Maxit, C. Yang, L. Cheng, and J.-L. Guyader. Modeling of micro-perforated panels in a complex vibro-acoustic environment using patch transfer function approach. *Journal of the Acoustical Society of America*, 131(3):2118–2130, 2012. [DOI].
11. L. Gallerand, M. Legrand, T. Dupont, and P. Leclaire. Vibration and damping analysis of a thin finite-size microperforated plate. *Journal of Sound and Vibration*, 541:117295, 2022. [DOI], [OA].
12. L. Gallerand, M. Legrand, T. Dupont, and P. Leclaire. Damping performance of finite microperforated plates using multi-sized and spacial distributions of perforations, 2023. Submitted in May 2023.
13. P. Leclaire, K.V. Horoshenkov, and A. Cummings. Transverse vibration of a thin rectangular porous plate saturated by a fluid. *Journal of Sound and Vibration*, 247(1):1–18, 2001. [DOI], [OA].
14. M.A. Biot. Theory of propagation of elastic waves in a fluid-saturated porous solid. I. Low-frequency range. *Journal of the Acoustical Society of America*, 28(2):168–178, 1956. [DOI], [OA].
15. J. Carbajo, J. Ramis, L. Godinho, and P. Amado-Mendes. Perforated panel absorbers with micro-perforated partitions. *Applied Acoustics*, 149:108–113, 2019. [DOI].
16. B. Zhang, S. Lang, P. Ge, and W. Zhuang. The study of sound absorption characteristic of micro-perforated panel with different diameter holes. In *29th International Congress and Exhibition on Noise Control Engineering (internoise 2000)*, 2000. [OA].